Journal of Cerebral Blood Flow & Metabolism (2015) 35, 1552–1560

www.jcbfm.com

RAPID COMMUNICATION

Micro-heterogeneity of flow in a mouse model of chronic cerebral hypoperfusion revealed by longitudinal Doppler optical coherence tomography and angiography

Vivek J Srinivasan[1], Esther Yu[2], Harsha Radhakrishnan[1], Anil Can[2], Mihail Climov[2], Conor Leahy[1], Cenk Ayata[2,3] and Katharina Eikermann-Haerter[2]

Although microvascular dysfunction accompanies cognitive decline in aging, vascular dementia, and Alzheimer's disease, tools to study microvasculature longitudinally *in vivo* are lacking. Here, we use Doppler optical coherence tomography (OCT) and angiography for noninvasive, longitudinal imaging of mice with chronic cerebral hypoperfusion for up to 1 month. In particular, we optimized the OCT angiography method to selectively image red blood cell (RBC)-perfused capillaries, leading to a novel way of assessing capillary supply heterogeneity *in vivo*. After bilateral common carotid artery stenosis (BCAS), cortical blood flow measured by Doppler OCT dropped to half of baseline throughout the imaged tissue acutely. Microscopic imaging of the capillary bed with OCT angiography further revealed local heterogeneities in cortical flow supply during hypoperfusion. The number of RBC-perfused capillaries decreased, leading to increased oxygen diffusion distances in the days immediately after BCAS. Linear regression showed that RBC-perfused capillary density declined by 0.3% for a drop in flow of 1 mL/100 g per minute, and decreases in RBC-perfused capillary density as high as 25% were observed. Taken together, these results demonstrate the existence of local supply heterogeneity at the capillary level even at nonischemic global flow levels, and demonstrate a novel imaging method to assess this heterogeneity.

Journal of Cerebral Blood Flow & Metabolism (2015) **35,** 1552–1560; doi:10.1038/jcbfm.2015.175; published online 5 August 2015

Keywords: angiography; capillary recruitment; Doppler optical coherence tomography; hypoperfusion; vascular dementia

INTRODUCTION

Chronic cerebral hypoperfusion induced by small-artery occlusion or critical arterial stenosis is a pathophysiologic hallmark of vascular dementia. Histologically characterized by white matter changes and multifocal infarctions, chronic cerebral hypoperfusion is associated with cognitive decline.[1–3] Rodent models of chronic cerebral hypoperfusion that use common carotid artery stenosis or occlusion mimic many aspects of vascular cognitive impairment in patients, including decreased cerebral blood flow, inflammation and blood–brain barrier abnormalities, brain atrophy, white matter degeneration, decreased metabolism, as well as impaired working memory.[4] Bilateral common carotid artery occlusion has been widely used in the rat to model chronic cerebral hypoperfusion.[5] Recently, mouse bilateral common carotid artery stenosis (BCAS) models have emerged.[6] In these models, although the degree of hypoperfusion is correlated with the extent of ischemic lesions and neurologic impairment,[7] the magnitude of flow reductions after BCAS were moderate at best (~30 to 40%),[8] at least relative to classic ischemic thresholds of 80 to 85%,[9–11] and lasted only a few days before collateral development and recovery of flow. The lack of classic ischemia raises questions about the precise mechanism of tissue loss and cognitive impairment. Previous studies have used laser Doppler flowmetry,[6–8] positron emission tomography,[8] and laser speckle flowmetry[8] to macroscopically monitor regional flow values after BCAS. However, critical changes in microvascular supply may not be reflected in regionally averaged blood flow values.

Doppler optical coherence tomography (OCT)[12] and optical microangiography[13] have been used to study ischemic stroke in mice, while optical microangiography was further used to study revascularization up to 4 weeks after penetrating brain trauma[14] in large vessels. Similar methods were used to study microischemia because of repeated cocaine administration[15] and to generate images of vasculature for longitudinal image registration in a mouse model of cerebral β-amyloidosis.[16] In this paper, we present an OCT platform that enables longitudinal and quantitative monitoring of both global flow and microvascular flow patterns during chronic cerebral hypoperfusion, imaged for up to nine time points in the same animal over 1 month. In particular, the system parameters, animal model, and scanning protocols were optimized to enable selective imaging of red blood cell (RBC)-perfused capillaries. Bilateral, thinned-skull, glass coverslip-reinforced cranial windows enabled capillary-scale resolution without perturbing cortical physiology. Cortical arteriolar blood flow, vessel diameter, and perfused capillary density were quantified using a range of scanning protocols and resolutions.

[1]Department of Biomedical Engineering, University of California Davis, Davis, California, USA; [2]Neurovascular Research Laboratory, Department of Radiology, Massachusetts General Hospital, Harvard Medical School, Charlestown, Massachusetts, USA and [3]Stroke Service and Neuroscience Intensive Care Unit, Department of Neurology, Massachusetts General Hospital, Harvard Medical School, Boston, Massachusetts, USA. Correspondence: Dr VJ Srinivasan, Department of Biomedical Engineering, University of California, Davis, 451 E Health Sciences Drive, GBSF 2521, Davis, California 95616, USA.
E-mail: vjsriniv@ucdavis.edu
Received 22 April 2015; revised 5 June 2015; accepted 19 June 2015; published online 5 August 2015

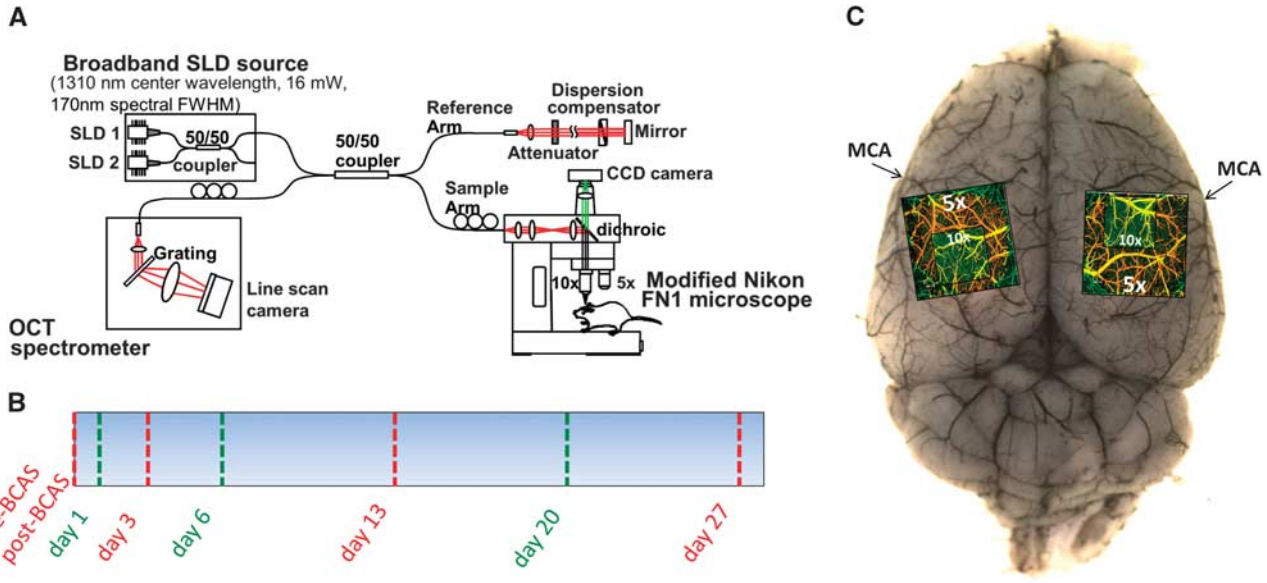

Figure 1. (**A**) Schematic of spectral/Fourier domain OCT system and microscope. (**B**) Timeline of imaging sessions. The pre- and post-BCAS imaging sessions occurred on day 0, one day after creation of cranial windows. Alternating imaging days are colored differently. (**C**) Overlay of OCT angiograms on a dorsal photograph of a carbon-black-perfused brain, showing fields of view that were imaged with each objective. BCAS, bilateral common carotid artery stenosis; MCA, middle cerebral artery; OCT, optical coherence tomography.

Our results show that while average flow in the imaged cortical regions remained mildly ischemic, rarefaction of the functional microvasculature (i.e., RBC-perfused capillaries) further compromised oxygen delivery, potentially creating ischemic microdomains. This observed 'micro-heterogeneity' of blood flow can explain previous observations of white matter degeneration, microinfarctions, and brain atrophy in the BCAS model, even as global flow reductions remained moderate. Our results suggest that the topology of the functional microvascular supply is a critical determinant of tissue degeneration and neurologic decline in global hypoperfusion states, and demonstrate a novel imaging method to assess this topology.

MATERIALS AND METHODS

Animal Preparation

Male, 24 to 29 g C57BL/6J mice ($N = 9$) from Charles River Lab (Wilmington, MA, USA) were used for these studies. Bilateral common carotid artery stenosis was induced in mice using 0.18 mm inner diameter steel coils (total length: 2.5 mm, Sawane Spring, Hamamatsu, Shizuoka Prefect, Japan).[6] Twenty-four hours before BCAS, bilateral, thinned-skull, glass coverslip-reinforced cranial windows[17] were created, overlying the middle and anterior cerebral artery watershed territory. Animals were allowed to recover overnight. The next day (day 0), baseline pre-BCAS imaging was performed, BCAS was induced, and post-BCAS imaging was performed. Each animal was imaged for a total of at least eight time points (immediately pre-BCAS, immediately post-BCAS, and 1 day, 3 days, 6 days, 13 days, 20 days, and 27 days after BCAS). In three mice, imaging was performed a ninth time on day 27 through a full craniotomy sealed with a glass coverslip. Mice were anesthetized with isoflurane (2.5% induction, 1 to 1.5% maintenance) in 80% air and 20% oxygen, and rectal temperature maintained at 37 °C using a homeothermic heating blanket for all imaging sessions. Longitudinal imaging precluded invasive blood pressure and heart rate monitoring until the last imaging session. For all other time points, anesthetic depth was titrated by an investigator experienced in monitoring the breathing rate and pattern to maintain optimal anesthetic depth during imaging. At the end of the imaging experiments, mice were perfused transcardially with carbon black. All the procedures were approved by the Subcommittee on Research Animal Care of Massachusetts General Hospital where these experiments were performed. All the experimental procedures and animal handling were performed according to the ARRIVE guidelines.

Optical Coherence Tomography System and Imaging

A 1,310 nm spectral/Fourier domain OCT microscope was constructed for *in vivo* imaging of the mouse cerebral cortex as shown in Figure 1. The light source consisted of two superluminescent diodes combined using a 50/50 fiber coupler to yield a bandwidth of 150 nm. The axial (depth) resolution was 4.8 μm in air (3.6 μm in tissue). The power on the sample was 4 mW, and the sensitivity was 103 dB. A spectrometer with a 1,024 pixel InGaAs line scan camera operated at 47,000 axial scans per second. Either a $\times 5$ objective or a $\times 10$ objective was used (Mitutoyo, Aurora, IL, USA), yielding a transverse resolution of either 7.2 or 3.6 μm, respectively.

Before each imaging time point (Figure 1B), mice were fixed in a custom-mounted stereotaxic frame that enabled adjusting head tilt along the rostrocaudal axis. The acquisition times for the OCT angiography and Doppler OCT protocols were approximately 2 minutes each. The imaging field of view was situated above the middle and anterior cerebral artery watershed region (Figure 1C). Including the time required for alignment (head tilt, translation, and focal depth), OCT imaging sessions required approximately 30 minutes per hemisphere.

Data Acquisition and Analysis

Angiography protocol. The OCT angiography[18] scanning protocol acquired frames (B-scans) with 512 axial scans repeated twice at each transverse *y*-location,[19] at a total of 5,120 transverse *y*-locations (10,240 frames). OCT angiography was performed over a

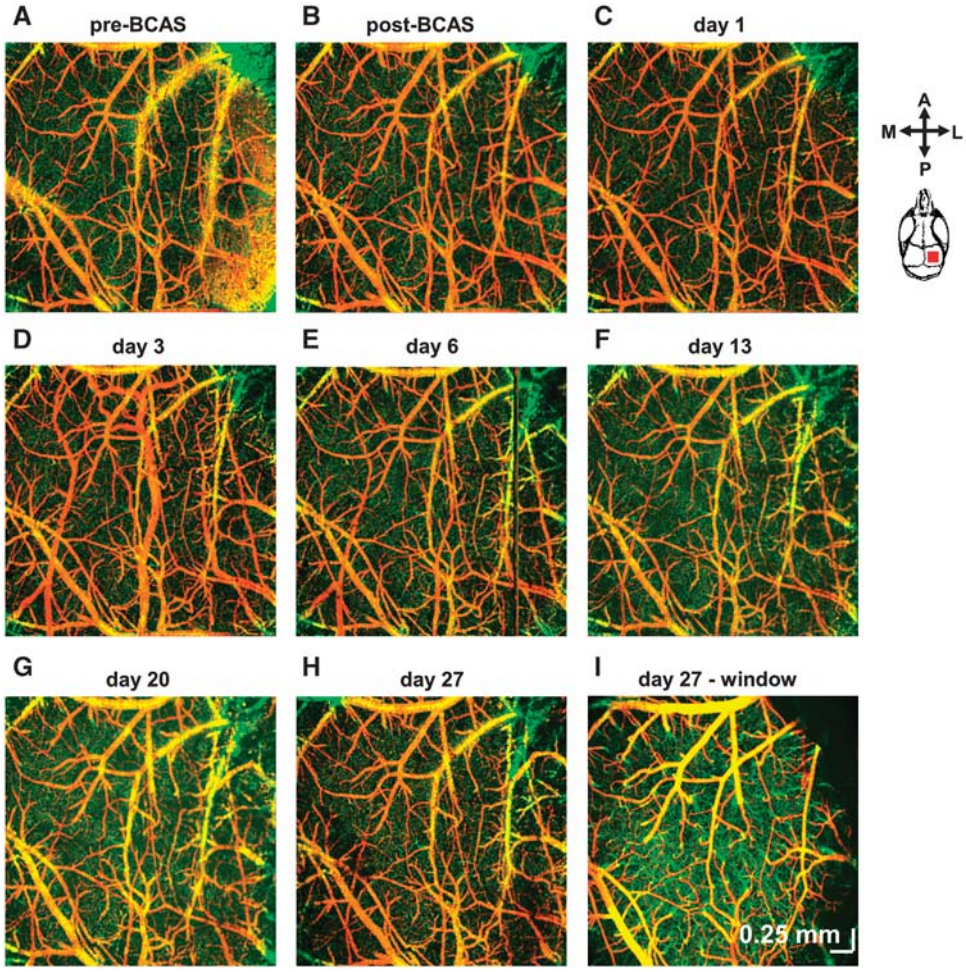

Figure 2. OCT angiography of longitudinal changes after bilateral common carotid artery stenosis (BCAS). Imaging was performed through the thinned-skull cranial window starting 1 day after window creation. Imaging was performed before BCAS (**A**), immediately after BCAS (**B**), and 1 day (**C**), 3 days (**D**), 6 days (**E**), 13 days (**F**), 20 days (**G**), and 27 days (**H**) after BCAS. On the last day, a full craniotomy was performed and imaging was performed through a cranial window closed with a glass coverslip (**I**). Data were obtained with ×5 objective. A, anterior; L, lateral; M, medial; OCT, optical coherence tomography; P, posterior.

cortical surface area of 3 mm × 3 mm (7.2 μm transverse resolution) or 1.0 × 1.0 mm (3.6 μm transverse resolution). To create angiogram frames, high-pass filtering was performed along the slow axis of repeated frames acquired at the same transverse location. For this protocol, the high-pass filtering operation amounted to a simple point-wise complex difference between two frames acquired at the same transverse *y*-location. Using a MATLAB graphical user interface, vessel diameters were manually calculated in arteries and veins from the angiograms. The identities of vessels (artery or vein) were determined from the OCT angiogram based on connectivity with larger vessels of a known type as well as morphology.[19] In Figure 2, example angiograms at each time point shown in Figure 1B from the lower transverse resolution (7.2 μm) data sets are shown for a single hemisphere, coloring superficial vessels yellow/orange and deeper capillaries green. Degradation of image quality is observed over the 1-month period, likely because of skull regrowth (Figures 2A–2H). In support of this observation, after skull and dura removal and implantation of a closed cranial window at 1 month, OCT angiograms revealed clear vascular morphology (Figure 2I).

Optical coherence tomography angiography selectively images red-blood-cell-perfused capillaries. On the basis of the high-resolution OCT angiography data, further analysis of blood-cell-perfused capillary distribution was performed. This analysis was based on the observation that the motion-based angiography technique effectively images only capillaries that are perfused by moving and scattering blood cells, a population that is dominated by RBCs under our experimental conditions. Assuming that perfusion with oxygen-carrying RBCs is necessary and sufficient for substantial oxygen delivery to the surrounding tissue; one may investigate the network of 'functional' capillaries that deliver oxygen to the surrounding tissue by simple image analysis of the OCT angiogram. Although previous work noted extreme functional capillary reduction in stroke[19] (Figure 3B), quantitative investigation of diffusion distance based on the concept of a blood-cell-perfused capillary network has not been performed.

As the angiogram depicts the number of capillaries perfused with moving blood cells, it is important to understand the effects of the discrete nature of RBC flux[20] on the imaging method. A necessary and sufficient condition for a capillary to be visualized in the angiogram is that at least one moving blood cell passes through a voxel during the observation time with a speed above the detection threshold. A capillary with extremely low flux or RBC speed will be missed by the scanning protocol, as illustrated in Figure 3. The minimum flux and speed requirements for detection are estimated in the sections below.

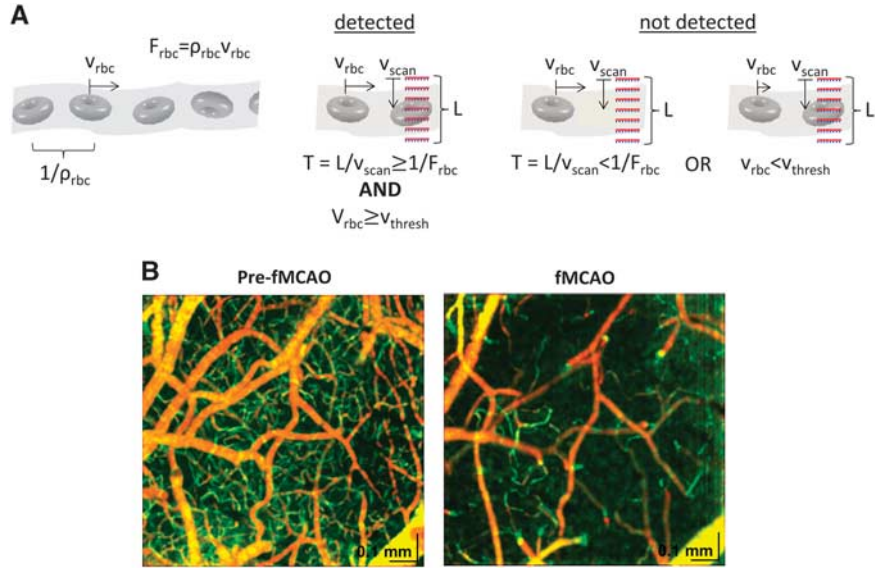

Figure 3. OCT angiography estimates RBC-perfused capillary density with a minimum detectible speed of 0.04 mm/second and a minimum detectable flux of ~1 cell/second. (**A**) Estimation of minimum detectable flux based on sampling a capillary. The angiography scan protocol resamples the same transverse location at intervals of 11 milliseconds (one even and one odd scan are required for a single angiography frame). The approximate condition for the detection of perfusion in a capillary is that at least one RBC passes during the transit time of the scan protocol across the capillary along the slow axis. The RBC speed must also exceed the speed threshold (thresh) for detection. (**B**) Example of extreme rarefaction of perfused capillaries during filament middle cerebral artery occlusion (fMCAO).[19] Data were obtained with ×10 objective. OCT, optical coherence tomography; RBC, red blood cell.

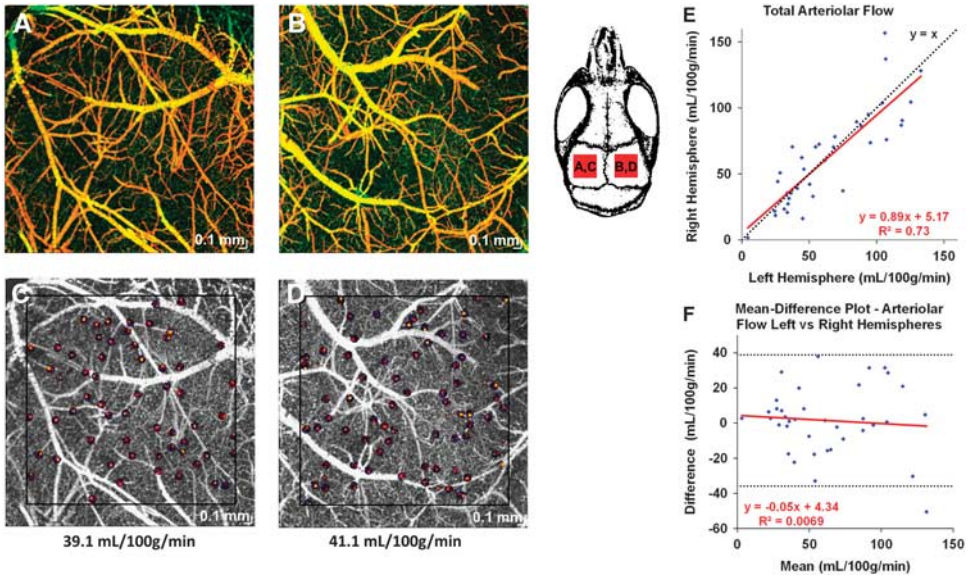

Figure 4. Bilateral comparison of cortical blood flow maps. Both hemispheres in an exemplary subject have vastly different vascular architectures, as evidenced by OCT angiography (**A** and **B**). Nevertheless, when arteriolar flow was summed over all vessels across the field of view (black square), comparable flow values (~40 mL/100 g per minute) were calculated (**C** and **D**). (**E**) Arteriolar flow in the left and right hemispheres shows good correlation across a range of subjects across time. (**F**) Mean-difference plot of arteriolar flow in the two hemispheres indicates agreement of the two measurements (95% limits of agreement shown as black dotted line), showing that consistent flow values are obtained, regardless of the feeding vascular architecture. Data were obtained with ×5 objective. OCT, optical coherence tomography.

Flux threshold: A single capillary parallel to the fast (x) axis of scanning would be sampled the fewest number of times by the protocol, and represents a worst-case scenario. First, assume that the extent of a capillary in the angiogram is on the order of $L = 7\,\mu$m for the ×10 objective (6 μm RBC diameter and 3.6 μm transverse resolution). The angiography scan protocol would resample that capillary 36 times over approximately $T = 0.8$ seconds, given 0.011 seconds per B-scan frame and 0.022 seconds per angiogram frame. The effective scan speed v_{scan} is thus approximately 9 μm/second. Thus, in this worst-case scenario, a capillary with an instantaneous flux F_{rbc} lower than $1/T = 1.3$ cell/second could be missed. (It is possible that an RBC with a speed $>7\,\mu$m/0.011 seconds = 0.64 mm/second may not be sampled; however, the stochastic non-periodic nature of RBC flux and dense sampling makes systematic missing of capillaries unlikely.) In general, for capillaries at an oblique angle to the fast

axis, such low fluxes could result in a 'patchy' appearance of the vascular network depending on the presence or absence of RBCs at the time and place at which a particular segment was sampled by our scan protocol. However, the image-enhancement step (discussed below) helps to reduce the patchy appearance of vessels, which may enable detection of capillaries even at fluxes of ~1 cell/second.

Speed threshold: In addition to the lower limit on the flux imposed by the scanning protocol, a lower speed limit for the OCT angiogram must be considered. The phase noise, caused by galvanometer jitter and physiologic motion, was determined to be a limiting factor in speed detection at the more superficial depths investigated here. The speed sensitivity of the angiography technique was estimated to be approximately 0.04 mm/second, based on the baseline decorrelation estimated from the phase noise of the system. Thus, any capillaries with blood cells moving at speeds < 0.04 mm/second (essentially stagnant) were not detected either.

The extremely low speed and flux thresholds calculated above justify our interpretation of the OCT-derived angiogram as depicting the functional capillary network that delivers substantial oxygen to the surrounding tissue. This analysis neglects the contribution of capillaries perfused solely with plasma; however, it may be argued that such vessels have a low capacity to deliver oxygen to surrounding tissue because of the low oxygen-carrying capacity of plasma alone.

Doppler protocol. Flow was calculated from Doppler OCT data by integration of the velocity axial (*z*) projection in the *en face* (*xy*) plane.[19] This procedure is based on the assumption that velocity represents an incompressible (zero divergence) vector field. Normalization to the estimated cortical mass was performed as described previously.[19] Three-dimensional Doppler OCT data sets were acquired over a cortical surface area of 2.5 mm × 2.5 mm with a transverse resolution of 7.2 μm. The Doppler OCT protocol consisted of four consecutive volumes of 256 frames with 4,096 axial scans each. Each volume required approximately 26 seconds, hence the Doppler OCT scanning protocol required approximately 2 minutes to complete. Doppler OCT frequency shifts were computed using adjacent axial scans along the fast axis of the frame; hence, the maximum measurable velocity axial projection, determined by the axial scan rate, was 11.4 mm/second. Care was taken to place the focus approximately 100 μm below the cortical surface. Using a custom-designed MATLAB graphical user interface, flow was calculated manually in individual vessels.

Figures 4A–4D show examples of angiography and absolute cortical arteriolar flow in the left and right hemispheres of the same animal immediately after BCAS. Figure 4E shows a scatter plot of the arteriolar flow in the left and right hemispheres of different animals at different time points. From the mean-difference plot in Figure 4F, flow values exhibit good agreement between the right and left hemispheres. The fact that relatively self-consistent results are obtained, although the two hemispheres typically have very different vascular supply patterns at the arteriolar level (e.g., Figures 4A–4D), supports the validity of this methodology.

Two-dimensional capillary analysis. From a maximum intensity projection angiogram of the entire data set at baseline (pre-BCAS), two to four regions of interest in the plane of the cortical surface devoid of large pial vessels were chosen. For each region of interest (ROI), two depths ranges corresponding to approximately 100 to 200 μm and 200 to 300 μm below the surface were chosen. A maximum intensity projection across each of these depth ranges was performed, generating two microvascular images. For each microvascular image, an automated program drew centerlines. Image enhancement was performed using a Hessian matrix-based approach to increase the contrast of vessel structures.[21] Adaptive thresholding of the enhanced image was then implemented to obtain a binary representation of the vasculature (i.e., an equivalent image with all vessel pixels set to 1, and all other pixels set to 0). Morphologic image processing was applied as an additional noise removal step. Vessel centerlines were then determined by using a thinning algorithm, which computed a one-pixel-thick subset of the binary vascular map.[22] Manual correction was performed to trace missing vessels and eliminate spurious vessels detected by the automated program. This process was repeated for all the time points up to day 6, by matching ROI locations and depth ranges to those established at baseline. One week after skull thinning, skull regrowth caused a degradation of resolution that precluded automated detection of capillaries. Moreover, evidence of angiogenesis and remodeling was seen at day 6, potentially complicating the interpretation of the capillary density determined from the angiograms. Therefore, capillary analysis was not continued beyond day 6. In the future, we anticipate that window removal and re-thinning of the skull may enable longitudinal imaging of capillary-level angiogenesis over longer time frames.

For all ROIs and maximum intensity projections, the perfused capillary density (units of per μm) was computed by dividing the total capillary length (units of μm) by the total area of the chosen ROI (units of μm^2). Densities from both maximum intensity projection images within each ROI were averaged. The resulting values were then averaged over all ROIs in a given hemisphere and normalized to the corresponding baseline (pre-BCAS) values.

Perfused capillary versus flow analysis. Lower flow values may correlate with lower perfusion pressures, and hence, capillary non-perfusion. To understand the relationship between flow and reduction in perfused capillary density, perfused capillary density was plotted against absolute flow values. When plotted against flow, capillary densities were normalized to the baseline (pre-BCAS) values for the same hemisphere. The baseline normalization procedure accounted for regional and between-subject differences in capillary density. Baseline values of normalized perfused capillary density were therefore equal to unity and this time point was excluded from the comparative analysis. A linear fit was performed to determine the relationship between flow and capillary density.

Three-dimensional capillary analysis and diffusion distance. A Krogh cylinder model is the simplest reductive model that incorporates the essential biophysics of oxygen diffusion from a capillary to be consumed in surrounding tissue. In this simplified model, each capillary exclusively supplies a well-defined region of surrounding tissue; thus, a fundamental parameter defining the maximum metabolic rate of oxygen that a given network topology can support is the Krogh cylinder radius or diffusion distance. Here, a three-dimensional (3D) representation of the functional microvasculature was used to compute an estimate of the distribution of distances from each tissue location to its nearest capillary. While this measure does not account for heterogeneity in flow and oxygenation in the perfused network, it coarsely reflects the capability of a given 3D microvascular topology (as defined by selectively imaged RBC-perfused capillaries) to deliver oxygen to tissue. Ascribing the determined average distance to a capillary to a 'diffusion distance' assumes that each tissue location is supplied exclusively by the nearest vessel, an assumption that is clearly incorrect. However, this simple analysis represents a first-order assay of changes in the functional network topology and the degree to which tissue regions are at risk because of sparser distribution of oxygen-supplying capillaries.

To assess diffusion distance, 3D analysis of the average distance from tissue voxels to the nearest vessel voxels versus depth was performed. A Euclidean distance transform was performed on a

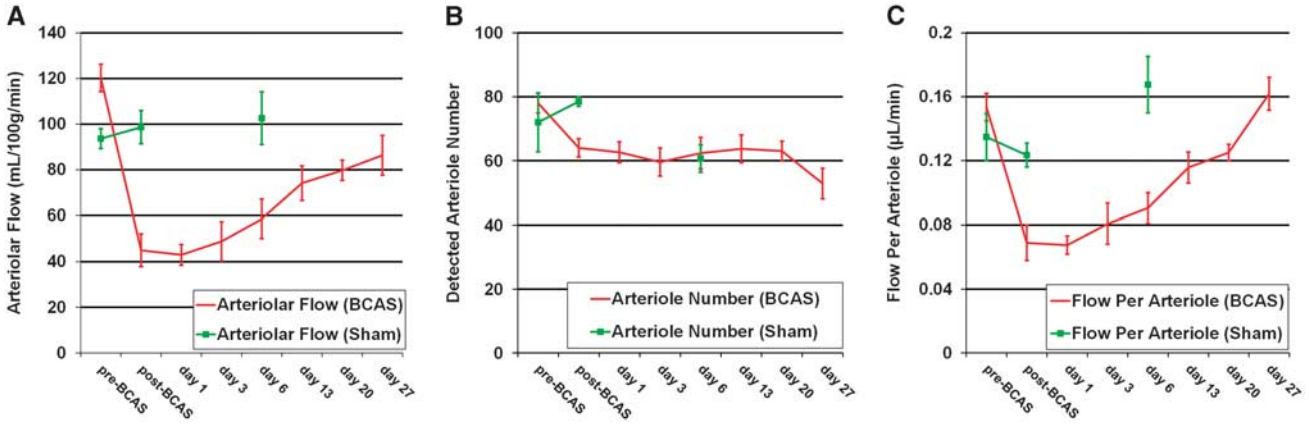

Figure 5. Longitudinal recovery of cortical blood flow was observed over the course of 1 month. (**A**) Arteriolar flow, converted to absolute units, dropped to 37% of baseline after BCAS and recovered to 72% of baseline by day 27. (**B**) The number of detected arterioles was also examined over time. A potential confound, evident from this plot, is that BCAS may have caused axial velocities in some arterioles to fall below the minimum detectable Doppler threshold. This would have reduced post-BCAS counts of arterioles, which were detected based on Doppler shifts. Another confound was skull regrowth at the edge of the imaged region, which led to a reduction in detected arteriole number over time, particularly at the last time point. Thus volumetric flow per arteriole was also examined. (**C**) The volumetric flow per arteriole dropped to 45% of baseline immediately after BCAS, and recovered to 105% of baseline by day 27. Sham animals subjected to surgical procedures without BCAS were imaged on day 0 and day 6 and included as controls ($N = 3$). Error bars are mean ± s.e.m. Data were obtained with ×5 objective. BCAS, bilateral common carotid artery stenosis.

binary vessel mask (obtained using a depth-dependent threshold after image enhancement). The mean of all non-zero values in the resulting 3D Euclidean distance map was determined. Predominantly, capillary volumes without overlying shadows of large vessels were chosen for the analysis, and volumes were precisely obtained by measuring depths from the skull surface, accounting for tilt. The accuracy of this method is limited by the fact that the segmented binary vascular mask is not a true volumetric representation of the extent of the blood vessels, and can only be regarded as an approximation.

RESULTS

Arteriolar flow (Figure 5), converted to absolute units by estimation of the mass corresponding to the underlying cortical volume, showed a drop of 63% after BCAS. Incomplete recovery was observed on day 27, with a persistent flow deficit of 28% relative to baseline. These results, showing a larger drop than previously reported,[8] are partially explained by the fact that detected arteriole number also showed a drop over time. The initial average detected arteriole number of 78 (Figure 5B) sourcing a cortical area of 6.25 mm^2 agrees well with the previous estimate of a cortical surface area of 0.09 mm^2 sourced by a penetrating arteriole, on average, in mice.[23] The initial drop in detected arteriole number to 64 after BCAS is most likely because of the drop in velocity in some arterioles below the minimum detectable Doppler frequency (determined by the scanning speed).[24] Similarly, total calculated venular flow, though highly correlated with arteriolar flow, may have been less than total arteriolar flow because of the lower venular velocity and hence, higher susceptibility of venules to velocity thresholding (Supplementary Figure 1). The drop between day 20 and day 27 is most likely because of skull regrowth at the edges of the window, which degrades Doppler signal-to-noise ratio.

By examining flow per arteriole (Figure 5C) instead, confounds related to the total arteriolar flow calculation were mitigated. When the flow per arteriole was plotted over time, the initial drop was found to be 55% after BCAS, and a complete flow recovery was observed, with the flow per arteriole on day 27 exceeding the flow per arteriole at baseline (pre-BCAS) by 5%. Moreover, flow per arteriole was found to be uncorrelated with total arteriole number (Supplementary Figure 2), although total arteriolar flow was correlated with total arteriole number. Relative changes in flow per arteriole are relatively consistent, though somewhat larger, than relative flow changes in the same model measured by laser Doppler flowmetry.[25] Nevertheless, flow, as assessed by Doppler OCT, remained well above classic ischemic thresholds.[9–11]

In some cases, angiography revealed remodeling of cortical vasculature (Supplementary Figure 3). Supplementary Figures 3A–3D demonstrate changes in vasculature at specific time points. There is clear growth of new vein branches on day 6 after BCAS (Supplementary Figure 3C) compared with baseline (Supplementary Figure 3A), potentially indicating angiogenesis. The same region shows possible refinement or pruning of branches by day 20 (Supplementary Figure 3D). In our hands, such clear observations of angiogenesis were anecdotal and only occurred when the flow drop after BCAS was particularly severe. Thus angiogenesis was not investigated further in this study. Because of angiogenesis around 1 week, capillary analysis was not continued past the 6-day time point. Angiogenesis of cortical vessels was not observed in sham animals.

Supplementary Figures 4A–4G show diameters at each time point relative to baseline (pre-BCAS) diameter for different vessel types (arteries, veins, collateral, and dura). Supplementary Figure 4H shows diameters over time (mean ± s.e.m. across vessels). Vessel diameters were measured at precisely corresponding cortical locations over time and compared with baseline (pre-BCAS, day 0) values. The diameters in Supplementary Figure 4H show that arteries exhibit slight initial reduction in diameter in the days following BCAS, followed by enlargement over weeks. By contrast, veins exhibit slight enlargement in the days following BCAS, followed by reduction in diameter over weeks, particularly in larger vessels. Collaterals, predominantly between the middle and posterior cerebral arteries, exhibit consistent growth over the month after BCAS (Supplementary Figure 4).

Capillary-level imaging (Figures 6A–6F) revealed further changes in micro-perfusion after BCAS. Though not as striking as in the core of a focal stroke (Figure 3B), an ~15 to 20% reduction in RBC-perfused capillary density relative to baseline occurred after BCAS (Figure 6G), with a larger reduction occurring for more severe drops in blood flow (Figure 6G). The slope of a linear fit of normalized perfused capillary density versus flow was 0.3%/(mL/

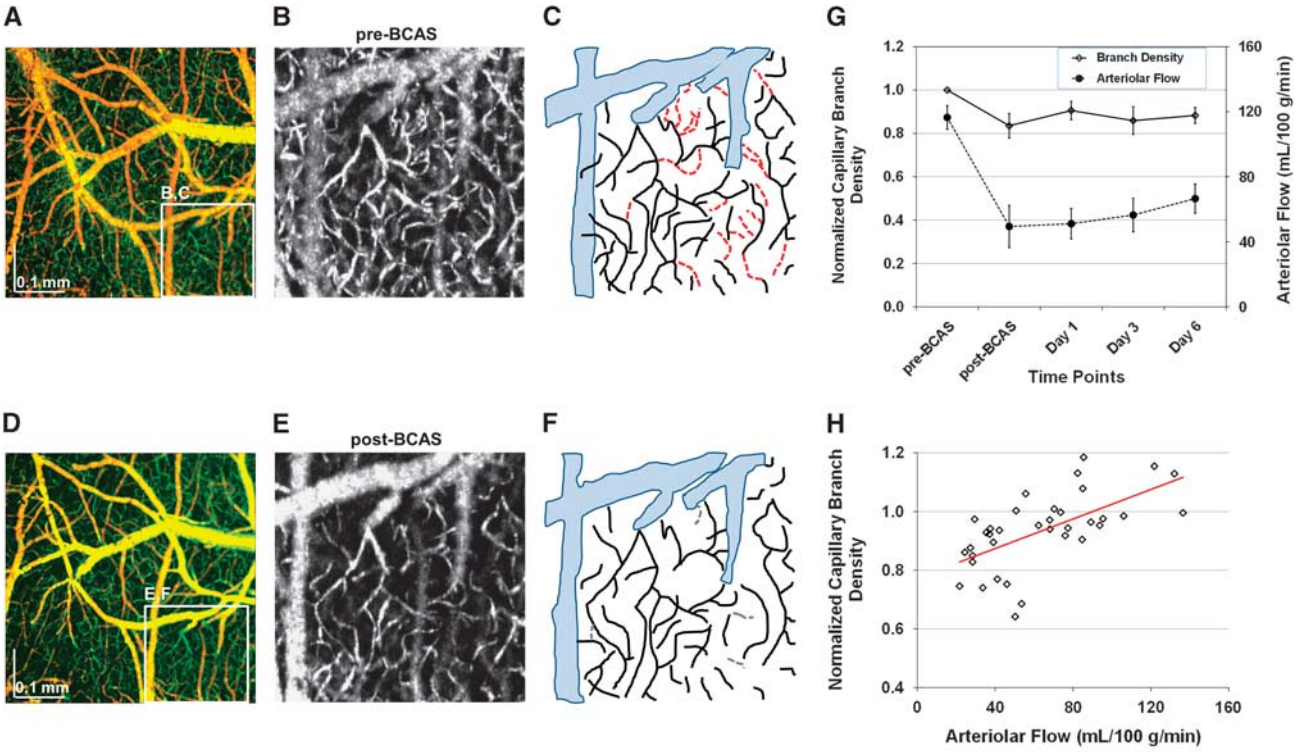

Figure 6. Capillary-level analysis demonstrates a profound reduction in the density of perfused capillaries in the early stages after BCAS. (**A** and **D**) The color-coded angiograms show a qualitative rarefaction of capillaries perfused with moving blood cells after BCAS. (**B** and **E**) Maximum intensity projections (MIPs) over 100 μm across the region of interest shown in **A** and **D**, starting approximately 100 μm below the surface, are shown. When capillary segments were directly tracked between time points, numerous capillary segments (red dotted segments in **C**) lost perfusion after BCAS. By comparison, the number of capillary segments that appeared after BCAS (gray dotted segments in **F**), most likely due to mis-registration, was small. (**G**) Perfused capillary branch density decreased alongside flow after BCAS, reaching a 15 to 20% reduction. (**H**) The perfused capillary density also decreas is flow, as shown by a linear fit (red line, $P < 0.0001$). This change in flow distribution at the capillary level may contribute to the development of microinfarcts, although flow changes were moderate. Data were obtained with $\times 10$ objective. BCAS, bilateral common carotid artery stenosis.

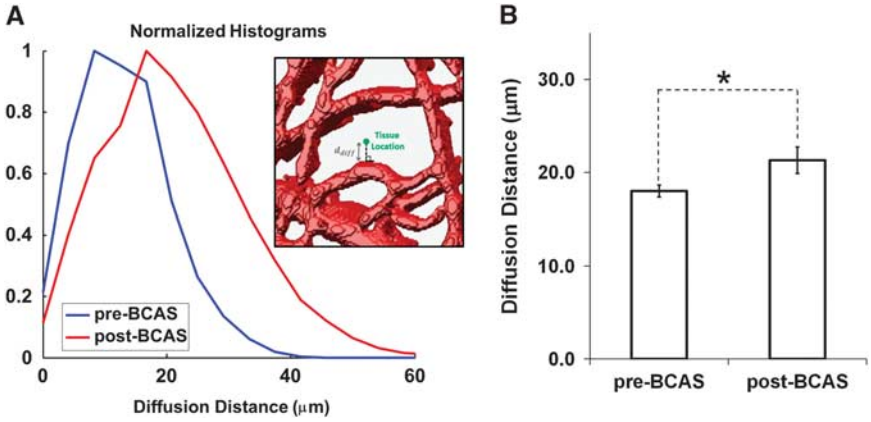

Figure 7. Tissue locations are significantly further, on average, from the nearest RBC-perfused capillary immediately after BCAS. (**A**) The histogram plot shows an increase in diffusion distances as well more spread in their distribution immediately after BCAS (red) compared with before BCAS (blue) in a single volumetric region from one animal. A rendering of the 3D RBC-perfused vascular network (after Hessian enhancement and thresholding) shows how diffusion distances is calculated for a sample tissue location (green dot, inset). (**B**) A bar plot of mean diffusion distance averaged over all hemispheres and animals ($N = 6$), determined over cortical depths ranging from 100 to 300 microns, shows a statistically significant difference after BCAS ($^*P < 0.05$). Data were obtained with $\times 10$ objective. BCAS, bilateral common carotid artery stenosis; RBC, red blood cell.

100 g per minute) (Figure 6H). Baseline (pre-BCAS) values of capillary density at each location were used to normalize subsequent measurements to account for regional and between-subject variations, but were otherwise not explicitly used in the fitting. A 3D analysis revealed that the more sparse RBC-perfused vasculature leads to a shift and spread in the distribution of tissue diffusion distances after BCAS (Figure 7A). When data were pooled across hemispheres and animals, a

statistically significant increase in the mean diffusion distance immediately after BCAS, relative to baseline, was discovered (Figure 7B).

Significant anatomic variations in the Circle of Willis are present in C57BL/6 mice, accounting for variability in outcomes for experimental models that use the common carotid arteries to target cerebral circulation.[26] For this set of studies, ventral photographs of carbon-black-perfused brains revealed that the posterior communicating artery was present either unilaterally or bilaterally in all mice except one.

CONCLUSIONS

Bilateral common carotid artery stenosis is frequently used as a model of chronic global cerebral hypoperfusion and mimicks vascular dementia. Compared with rat bilateral common carotid artery occlusion models, the mouse BCAS model[5] enables behavioral testing because of preservation of the visual system, and facilitates mechanistic transgenic studies. Although flow in the BCAS model has been characterized with techniques such as laser Doppler flowmetry,[7,25] this method cannot directly assess blood flow heterogeneity within microdomains. Here, using a novel OCT imaging platform, we demonstrate decreased RBC-perfused capillary paths in the superficial cortex that accompany the previously described global reduction in cerebral blood flow values. More importantly, the distribution of distances from tissue to the nearest capillary rises significantly during hypoperfusion (Figure 7). The increase in diffusion distance may impact tissue oxygenation, possibly explaining the observation of microinfarctions at seemingly non-injurious global cerebral blood flow levels.

Microvasculature remains largely inaccessible to macroscopic imaging techniques such as MRI. Therefore, microscopic methods are needed to interrogate microvascular function in pathophysiology. However, conventional two-photon and confocal microscopy models that use cranial windows are invasive and capillary-scale measurements are cumbersome.[27,28] Here, we imaged arteriolar supply and density of RBC-perfused capillaries longitudinally without exposing the cortex. With an extremely low threshold for detection of RBC perfusion (0.04 mm/second or 1 cell/second), dropout of capillaries from the functional network of oxygen delivery immediately after BCAS was shown. This topological change in the oxygen-delivering capillary network (Figure 6) is an extreme form of heterogeneity[29,30] that increases the average effective diffusion distance for oxygen (Figure 7). Thus, capillary dropout (the opposite of recruitment[27]) occurs during cerebral hypoperfusion.

Although results show that RBC-perfused capillary dropout occurs in the BCAS mouse model, they do not address whether this represents an epiphenomenon of the reduced perfusion pressure. The question of whether the dropout is a consequence of exclusion of cells from plasma-only perfused paths, complete capillary collapse, or leukocyte plugging remains to be investigated using other more specific labeling approaches.[31] The potential role of factors such as edema or active pericyte constriction[32] should also be explored. Last, our data suggest that prominent changes in RBC-perfused capillary density were present mainly below a threshold flow of around 60 mL/100 g per minute (Figure 6H). However, the present study was not designed to distinguish between the linear relationship (Figure 6H) and a 'broken stick' that could have modeled such a threshold effect.

The findings are also qualified by the use of isoflurane anesthesia, which causes vasodilation even at the low levels (1 to 1.5%) used here. For this reason, the capillary dropout phenomenon should be studied further under different anesthetics, and in awake and behaving animals. The vessel diameters in Supplementary Figure 4 point to the potential effects of isoflurane anesthesia. The venous dilation observed in this study after BCAS is in agreement with a recent longitudinal imaging study in awake, behaving mice after unilateral common carotid artery occlusion.[33] However, the slight initial arterial constriction relative to baseline (excluding collaterals) observed after BCAS in the present study contrasts with prominent arterial dilation relative to baseline observed after unilateral carotid artery occlusion in awake, behaving mice.[33] These differences are most likely because of anesthesia, but may also result, in part, from the larger degree of hypoperfusion in the BCAS model. Had this study been conducted in awake mice, we hypothesize that we would have observed arterial dilation similar to that observed in the carotid artery occlusion model.[33]

Beyond investigation of the BCAS model, the extensive data set generated by this study also afforded several opportunities for methodological validation. Bilateral agreement of global cortical blood flow values (Figure 4) determined from arterioles suggested consistency of the Doppler OCT quantification method, even though vascular architecture differed greatly between hemispheres. Correlation of arteriolar and venular flows was also demonstrated (Supplementary Figure 1). However, the systematic difference between arteriolar and venular flows, particularly at low flow values, suggested that a Doppler velocity threshold effect was present in venules. A similar effect is observed in Doppler ultrasound.[34] Thus, caution should be exercised in interpreting very low flow values or those obtained under low signal-to-noise conditions (e.g., through a thick skull), even in arterioles. With these caveats, relative changes in flow per arteriole (Figure 5C) determined in this study agreed reasonably well with laser Doppler results from prior studies.[7,25]

In conclusion, we developed a novel, robust imaging platform for longitudinal imaging of hemodynamic recovery during chronic cerebral hypoperfusion in the mouse neocortex after BCAS. Recovery was imaged for up to 1 month. Although global flow values remained mildly ischemic, microinfarcts and brain atrophy have been routinely reported in the BCAS model. By using an OCT angiography protocol tailored for selective imaging of RBC-perfused capillaries, we show that this apparent discrepancy can be explained by micro-heterogeneities in cortical blood flow supply at the capillary level, which likely compromises oxygen delivery in the early days of hypoperfusion. These results highlight that pathologic microscopic perfusion patterns may lead to ischemia in local microdomains, even at global flow levels above conventional ischemic thresholds.

AUTHOR CONTRIBUTIONS

VJS, CA, and KE-H conceived and designed the experiments; VJS, EY, AC, MC, and KE-H performed the experiments; VJS, HR, AC, and CL analyzed the data; VJS, HR, CL, CA, and KE-H wrote and edited the manuscript; all the authors reviewed the manuscript before publication.

DISCLOSURE/CONFLICT OF INTEREST

The authors declare no conflict of interest.

ACKNOWLEDGMENTS

We thank Maria Angela Franceschini, Michael Moskowitz, and Bruce Rosen for general support. We thank Yahya Atalay and Andrea Negro for assistance with data analysis. We acknowledge support from the National Institutes of Health (VJS: NS067050; CA: NS061505, NS055104), the American Heart Association (VJS: IRG5440002; KE-H: 10SDG2610275), the Glaucoma Research Foundation Catalyst for a Cure (VJS), The Massachusetts General Hospital Claflin Distinguished Award, and Fondation Leducq (CA), The Heitman Foundation (CA), and The Ellison Foundation (CA).

REFERENCES

1 Iadecola C. Neurovascular regulation in the normal brain and in Alzheimer's disease. *Nat Rev Neurosci* 2004; **5**: 347–360.
2 Iadecola C. The pathobiology of vascular dementia. *Neuron* 2013; **80**: 844–866.

3 Prince M, Patel V, Saxena S, Maj M, Maselko J, Phillips MR *et al*. No health without mental health. *Lancet* **370**: 859–877.
4 Jellinger KA. Pathology and pathogenesis of vascular cognitive impairment—a critical update. *Front Aging Neurosci* 2013; **5**: 17.
5 Farkas E, Luiten PG, Bari F. Permanent, bilateral common carotid artery occlusion in the rat: a model for chronic cerebral hypoperfusion-related neurodegenerative diseases. *Brain Res Rev* 2007; **54**: 162–180.
6 Shibata M, Ohtani R, Ihara M, Tomimoto H. White matter lesions and glial activation in a novel mouse model of chronic cerebral hypoperfusion. *Stroke* 2004; **35**: 2598–2603.
7 Miki K, Ishibashi S, Sun L, Xu H, Ohashi W, Kuroiwa T *et al*. Intensity of chronic cerebral hypoperfusion determines white/gray matter injury and cognitive/motor dysfunction in mice. *J Neurosci Res* 2009; **87**: 1270–1281.
8 Nishio K, Ihara M, Yamasaki N, Kalaria RN, Maki T, Fujita Y *et al*. A mouse model characterizing features of vascular dementia with hippocampal atrophy. *Stroke* 2010; **41**: 1278–1284.
9 Astrup J, Siesjo BK, Symon L. Thresholds in cerebral ischemia - the ischemic penumbra. *Stroke* 1981; **12**: 723–725.
10 Astrup J, Symon L, Branston NM, Lassen NA. Cortical evoked potential and extracellular K+ and H+ at critical levels of brain ischemia. *Stroke* 1977; **8**: 51–57.
11 Branston NM, Strong AJ, Symon L. Extracellular potassium activity, evoked potential and tissue blood flow. Relationships during progressive ischaemia in baboon cerebral cortex. *J Neurol Sci* 1977; **32**: 305–321.
12 Yu L, Nguyen E, Liu G, Choi B, Chen Z. Spectral Doppler optical coherence tomography imaging of localized ischemic stroke in a mouse model. *J Biomed Opt* 2010; **15**: 066006.
13 Jia Y, Wang RK. Optical micro-angiography images structural and functional cerebral blood perfusion in mice with cranium left intact. *J Biophotonics* 2011; **4**: 57–63.
14 Jia Y, Grafe MR, Gruber A, Alkayed NJ, Wang RK. *In vivo* optical imaging of revascularization after brain trauma in mice. *Microvasc Res* 2011; **81**: 73–80.
15 Ren H, Du C, Yuan Z, Park K, Volkow ND, Pan Y. Cocaine-induced cortical microischemia in the rodent brain: clinical implications. *Mol Psychiatry* 2012; **17**: 1017–1025.
16 Bolmont T, Bouwens A, Pache C, Dimitrov M, Berclaz C, Villiger M *et al*. Label-free imaging of cerebral beta-amyloidosis with extended-focus optical coherence microscopy. *J Neurosci* 2012; **32**: 14548–14556.
17 Drew PJ, Shih AY, Driscoll JD, Knutsen PM, Blinder P, Davalos D *et al*. Chronic optical access through a polished and reinforced thinned skull. *Nat Methods* 2010; **7**: 981–984.
18 Wang RK, Jacques SL, Ma Z, Hurst S, Hanson SR, Gruber A. Three dimensional optical angiography. *Opt Express* 2007; **15**: 4083–4097.
19 Srinivasan VJ, Mandeville ET, Can A, Blasi F, Climov M, Daneshmand A *et al*. Multiparametric, longitudinal optical coherence tomography imaging reveals acute injury and chronic recovery in experimental ischemic stroke. *PLoS One* 2013; **8**: e71478.
20 Ren H, Du C, Park K, Volkow ND, Pan Y. Quantitative imaging of red blood cell velocity *in vivo* using optical coherence Doppler tomography. *Appl Phys Lett* 2012; **100**: 233702–2337024.
21 Frangi AF, Niessen WJ, Vincken KL, Viergever MA. Multiscale vessel enhancement filtering. In: *Medical Image Computing and Computer-Assisted Intervention-MICCAI*. Springer: Berlin/Heidelberg, Germany, 1998; pp 130–137.
22 Tsai PS, Kaufhold JP, Blinder P, Friedman B, Drew PJ, Karten HJ *et al*. Correlations of neuronal and microvascular densities in murine cortex revealed by direct counting and colocalization of nuclei and vessels. *J Neurosci* 2009; **29**: 14553–14570.
23 Blinder P, Shih AY, Rafie C, Kleinfeld D. Topological basis for the robust distribution of blood to rodent neocortex. *Proc Natl Acad Sci USA* 2010; **107**: 12670–12675.
24 Tao YK, Davis AM, Izatt JA. Single-pass volumetric bidirectional blood flow imaging spectral domain optical coherence tomography using a modified Hilbert transform. *Opt Express* 2008; **16**: 12350–12361.
25 Ihara M, Tomimoto H. Lessons from a mouse model characterizing features of vascular cognitive impairment with white matter changes. *J Aging Res* 2011; **2011**: 978761.
26 Doyle KP, Fathali N, Siddiqui MR, Buckwalter MS. Distal hypoxic stroke: a new mouse model of stroke with high throughput, low variability and a quantifiable functional deficit. *J Neurosci Methods* 2012; **207**: 31–40.
27 Villringer A, Them A, Lindauer U, Einhaupl K, Dirnagl U. Capillary perfusion of the rat brain cortex. *Circ Res* 1994; **75**: 55–62.
28 Kleinfeld D, Mitra PP, Helmchen F, Denk W. Fluctuations and stimulus-induced changes in blood flow observed in individual capillaries in layers 2 through 4 of rat neocortex. *Proc Natl Acad Sci USA* 1998; **95**: 15741–15746.
29 Jespersen SN, Ostergaard L. The roles of cerebral blood flow, capillary transit time heterogeneity, and oxygen tension in brain oxygenation and metabolism. *J Cereb Blood Flow Metab* 2012; **32**: 264–277.
30 Ostergaard L, Aamand R, Gutierrez-Jimenez E, Ho YC, Blicher JU, Madsen SM *et al*. The capillary dysfunction hypothesis of Alzheimer's disease. *Neurobiol Aging* 2013; **34**: 1018–1031.
31 Masamoto K, Takuwa H, Seki C, Taniguchi J, Itoh Y, Tomita Y *et al*. Microvascular sprouting, extension, and creation of new capillary connections with adaptation of the neighboring astrocytes in adult mouse cortex under chronic hypoxia. *J Cereb Blood Flow Metab* 2014; **34**: 325–331.
32 Yemisci M, Gursoy-Ozdemir Y, Vural A, Can A, Topalkara K, Dalkara T. Pericyte contraction induced by oxidative-nitrative stress impairs capillary reflow despite successful opening of an occluded cerebral artery. *Nat Med* 2009; **15**: 1031–U82.
33 Tajima Y, Takuwa H, Kokuryo D, Kawaguchi H, Seki C, Masamoto K *et al*. Changes in cortical microvasculature during misery perfusion measured by two-photon laser scanning microscopy. *J Cereb Blood Flow Metab* 2014; **34**: 1363–1372.
34 Osmanski BF, Martin C, Montaldo G, Laniece P, Pain F, Tanter M *et al*. Functional ultrasound imaging reveals different odor-evoked patterns of vascular activity in the main olfactory bulb and the anterior piriform cortex. *Neuroimage* 2014; **95**: 176–184.

Supplementary Information accompanies the paper on the Journal of Cerebral Blood Flow & Metabolism website (http://www.nature.com/jcbfm)